AIAA 96-3194

Channel Length and Thruster Performance of Hall Thrusters

K. Komurasaki, K. Mikami and D. Kusamoto
Nagoya university
Nagoya, Japan

32nd AIAA/ASME/SAE/ASEE
Joint Propulsion Conference
July 1-3, 1996 / Lake Buena Vista, FL

CHANNEL LENGTH AND THRUSTER PERFORMANCE OF HALL TURUSRTERS

Kimiya KOMURASAKI*, Kenji MIKAMI†, and Daisuke, KUSAMOTO†
Department of Aerospace Engineering
Nagoya University
Chikusa, Nagoya 464-01, Japan

Abstract

Optimization of the channel length for non-SPT type Hall thrusters is discussed. The optimum channel length was experimentally investigated with a channel-variable Hall thruster. In the case of the argon propellant, maximum beam-current has been extracted at the channel length, L = 4 mm. From a theoretical study based on a simple plasma discharge model, the optimum length is expressed by a function of the neutral mean free-path and the channel width.

Nomenclature

B : magnetic induction, T
e : electronic charge, C
I_b : ion-beam current, A
I_e : electron current at the channel exit, A
I_d : discharge current, A
I_p : ion production current, A
j : current density, A/m^2
L_{loss} : ion-loss characteristic length, m
L : channel length, m
m : electron mass, kg
$\dot{m}$: mass flowrate, kg/sec
M : atomic mass, kg
n : number density, m^{-3}
r : distance from the thruster exit, m
S : channel cross section area, m^2
T : temperature, K
v : velocity, m/sec
V_a : discharge voltage, V
V_{ion} : first ionization energy, eV
W : channel width, m
z : axial position in the channel, m
α : ion-loss fraction
β : ion-production coefficient
γ^2 : thrust coefficient
μ : electron mobility, m/Vsec
λ : mean free-path, m
η_a : acceleration efficiency, I_b/I_d
η_T : thrust efficiency
η_E : beam energy efficiency
η_u : propellant utilization efficiency, $I_b/(e\dot{m}/M)$
σ : collision cross-section, m^2
χ : channel configuration parameter

Subscript
e : electron
i : ion
n : neutral

---

* Assistant Professor, Member AIAA
† Graduate Student

Introduction

A Hall thruster, which is one of the electrostatic accelerators, can produce higher thrust density than conventional electrostatic thrusters, because the acceleration channel is filled with quasi-neutral plasma and there is no space-charge limited current. Furthermore, it can operate in the wide I_{sp} range by choosing discharge voltages and propellant gases. Because of these advantages, the Hall thruster is thought useful for applications to near earth missions.[1,2]

However, it still has some problems to be overcome. The first is its low thrust efficiency compared with the conventional electrostatic thrusters. The second is the insulator erosion due to the ion sputtering, which limits the thruster life-time.[3-5] The third is the large exhaust-beam divergence, which causes the electrostatic charging and the communication interference of satellites.[6]

As for the thrust efficiency, it can be expressed by the products of three internal efficiencies as $\eta_T = \gamma^2\eta_a\eta_u\eta_E$.[7] η_E (the ratio of the average beam-ion energy to the acceleration voltage) is 0.6 - 0.8 for most of the thrusters and for various operating conditions. η_u is almost unity when the propellant is xenon. η_a varies from 0.3 to 0.8 depending on the channel design. Therefore, η_a is focused on in this study.

In our previous researches,[8,9] it was found that the channel length is one of the most important design

both the ionization and the wall-loss processes. The optimum channel length is thought to be determined from the balance between the ion-production rate and the ion-loss rate in the channel. The objective of this research is to get the information about the design-criteria of the channel length for the good thruster performance by means of experiments and theoretical considerations.

Experimental apparatus and methods

A channel-variable Hall thruster is shown in Fig. 1. It has an acceleration channel insulated with two ceramic cylinders. The inner and outer diameter of the channel are 36 mm and 48 mm, respectively. An anode is located at the upstream end of the channel and has twenty small apertures to feed the propellant gas uniformly into the channel. The channel length is variable from 1.5 to 10 mm by changing the anode-ring width. A solenoidal coil is set at the center of the thruster to apply the magnetic fields in the radial direction in the channel. The magnetic induction is almost constant through the channel. This magnetic field configuration is different from that of the Russian SPT-type Hall thrusters, whose magnetic fields have a peak at the channel exit.

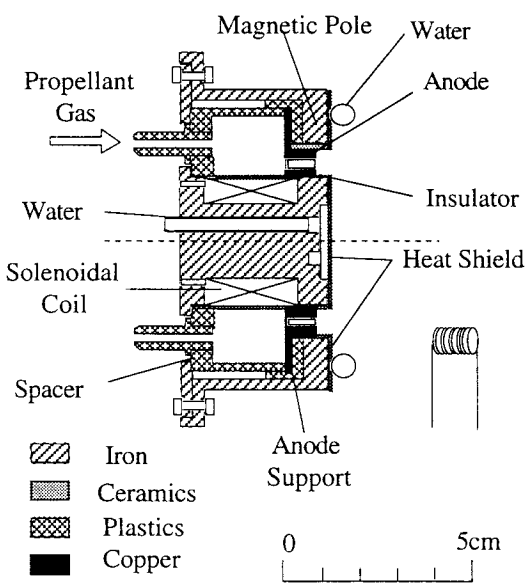

Fig. 1 A channel-variable Hall Thruster.

Xenon, krypton and argon are tested as a propellant gas. Propellant mass flow is regulated using a thermal mass-flow controller. A filament cathode, which supplies electrons to sustain the discharge and to neutralize the ion beam, is used instead of a hollow cathode for operation convenience. The filament is made of 2% thoriated tungsten wires coated with the double-carbonate powder to reduce its work function for electron emission.

The vacuum chamber is 1.0 m diameter and 1.6 m long. It is evacuated by two diffusion pumps backed by a roots blower and a rotary pump. The total pumping speed is 10000 l/sec. The back-pressure was maintained in the order of 10^{-4} Torr during the operation. Three power supplies (for main discharge, solenoidal-coil excitation and cathode heating) are used. In order to stabilize the discharge, 20 Ω resistor is added to the main discharge circuit. It takes a few minutes for the main discharge to be stabilized.

A multi-ion-collector system is used for the beam-current measurement. Seven ion-collectors are set on an arc-shape stage surrounding the thruster at a radius of 20, 30 and 40 cm as shown in Fig. 2. Each collector, which consists of a copper plate (2 cm x 5 cm) and a ceramic support, is biased to – 30 V, pointing at the center of the thruster exit. (The cathode is grounded.)

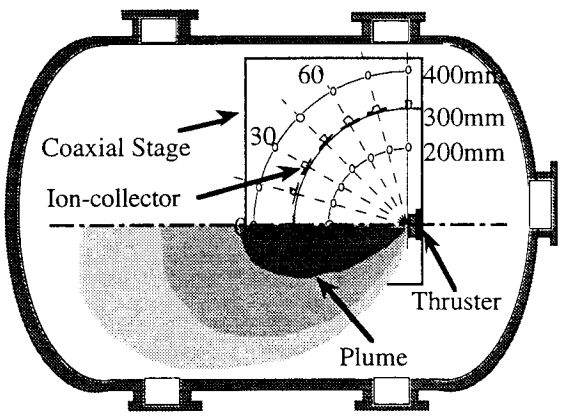

Fig. 2 Beam-current measurement system.

The total beam-current, $I_b(r)$, is obtained by means of the hemispherical integration of the measured angular current density distribution.

$$I_b(r) = \int_0^{\pi/2} j(r,\theta) 2\pi r \sin\theta \, r d\theta \qquad (1)$$

Experimental results

In Fig. 3, the measured total beam-current is plotted as a function of the distance from the collector to the thruster. It decreases with the distance due to the resonant charge-exchange collisions between ions and neutral particles in a vacuum chamber.[10-13] The solid line is the exponential curve fitting of the measured data. Theoretically, the total beam-current, $I_b(r)$ is expressed as

$$I_b(r) = I_{b0} \exp(-r/\lambda_i) \qquad (2)$$

where λ_i is the ion mean free-path for the charge exchange reaction, and identical to $v_i/n_n\langle\sigma_{ce}v_i\rangle$. ($\sigma_{ce}$ is the resonant charge-exchange cross section.) I_{b0} is the total beam current at the thruster exit, which is necessary for evaluating η_a and η_u. Table 1 shows λ_i obtained from the curve fitting of experimental data and the one from theoretical prediction. Since the comparison shows a good agreement, it is concluded that I_{b0} can be precisely estimated from Eq. (2) even when the back pressure is in the order of 10^{-4} Torr.

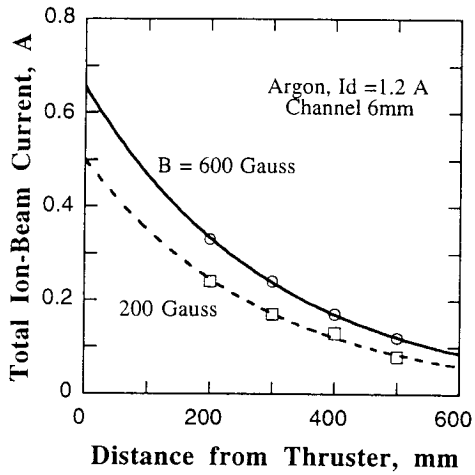

Fig. 3 Measured total ion-beam current.

Table 1 Ion mean free-path for charge exchange reaction. p_n = 8 x10^{-4} Torr, T_n = 300 K, kT_i = 100 eV.

Curve fitting	(B =200 G)	325 mm
	(B =600 G)	305 mm
Theory		300 mm

Figure 4 shows the relationship between the channel length and the acceleration efficiency. In the case of the argon propellant, maximum efficiency is marked at the channel length L = 4 mm, whereas in the case of krypton or xenon propellant, the efficiency decreases monotonously with the channel length. The optimum length seems to be less than 4 mm for these gases.

The effect of magnetic induction on the acceleration efficiency is shown in Fig. 5. The optimum channel length does not change with the magnitude of magnetic induction, while the efficiency itself increases with the magnitude of induction.

Figure 6 shows a plot of the measured discharge voltage vs. BL. The linear relationship indicates that the $1/B$ diffusion (Bohm diffusion) coefficient is more appropriate than the $1/B^2$ classical diffusion coefficient to describe the electron motion in our thruster. The discharge voltage became relatively low because the mass-flow rate had been set larger and the discharge current smaller than normal operating condition, to operate the thruster for various channel length and magnetic induction at the same mass-flow rate and discharge current.

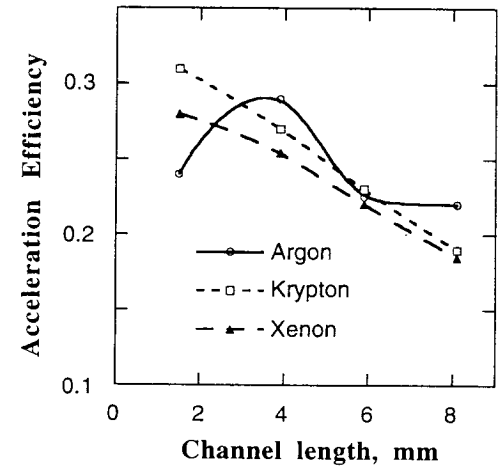

Fig. 4 Acceleration efficiency and channel length for various propellant gas.

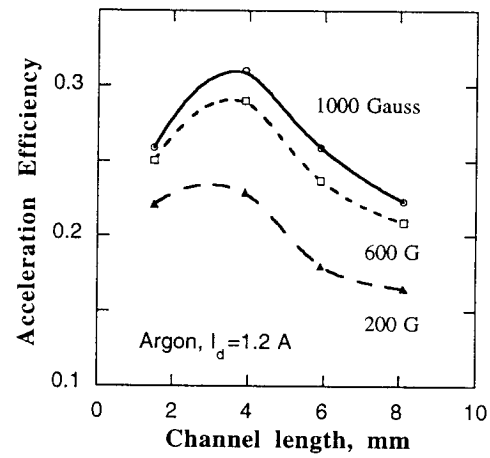

Fig. 5 Acceleration efficiency and channel length for various magnetic induction.

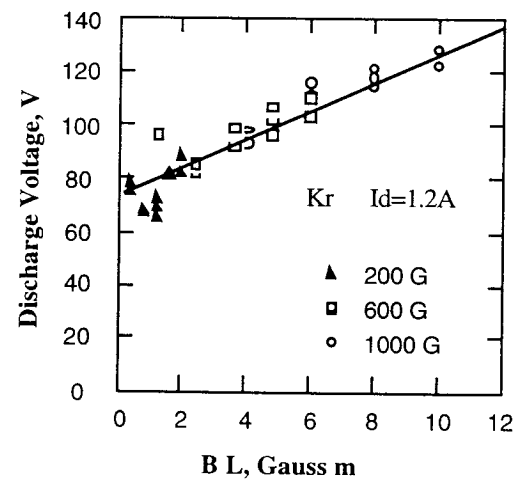

Fig. 6 Discharge voltage vs. BL.

Plasma discharge model

The acceleration efficiency is written by a function of the ion-loss fraction and the ion-production coefficient.

$$\eta_a = (1 - \alpha)\beta \qquad (3)$$

Here, α is defined as the ratio of the ions lost to the walls that produced in the channel, $(I_p - I_b)/I_p$, and β is defined as the ratio of the total ion-production rate to the discharge current, I_p/I_d. Both the ion-production and ion-loss rates are strongly affected by the channel length. Therefore, let's express these coefficients as a function of the channel length.

Ion-loss fraction

The electric fields in the acceleration channel are mainly aligned in the axial direction. However, they are distorted toward the channel wall[8,9] due to the magnetic-field curvature, electron-density gradients, and the pre-sheath made on the wall surface as schematically shown in Fig. 7. In a practical thruster design, these electric-field distortions are inevitable.

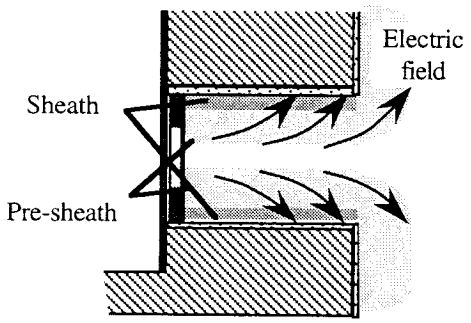

Fig. 7 Electric field distortion.

The ion-loss is caused by the radial component of the distorted electric fields. Figure 8 shows the typical ion-extraction cone and ion-loss envelope in the channel, which configuration has been known from the probe diagnostics and from the two-dimensional numerical simulations.[8,9]

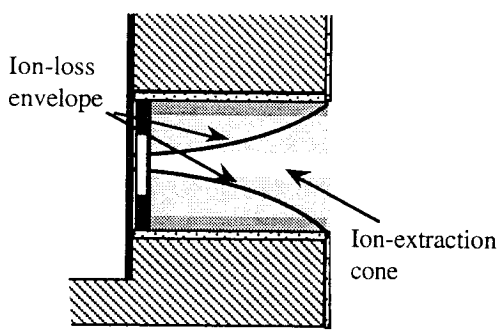

Fig. 8 Ion-extraction cone and ion-loss envelope.

By approximating the ion-loss envelope by an exponential function, the ion-loss fraction can be expressed as a function of the channel length as

$$\alpha = 1 - \exp(-L / L_{loss}) \qquad (4)$$

Here, the ion production rate is assumed uniform in the channel. L_{loss} is a characteristic length for the ion-loss envelope. From the scaling consideration, L_{loss} should be proportional to the channel width.

$$L_{loss} = \chi W \qquad (5)$$

χ varies with the channel geometry: For example, in the case of a rectangular channel, it is close to unity, while it becomes larger when the channel cross section is diverging toward the exit.

Ion-production coefficient

The electron-impact ionization is the dominant ion-production mechanism in the channel. Therefore, total ion-production current in the channel is expressed as

$$I_p = \int_0^L e n_n n_e \langle \sigma v \rangle S \, dz \qquad (6)$$

From the continuity of the neutral particles, the neutral density in the channel can be written as

$$n_n = (\dot{m} / M v_n) \exp(-z / \lambda_n) \qquad (7)$$

Here, λ_n is the neutral mean free path for the ionization reaction.

$$\lambda_n = v_n / n_e \langle \sigma v \rangle \qquad (8)$$

Substituting Eqs. (7) and (8) into Eq. (6), the ion-production coefficient is expressed by a function of the channel length as

$$\beta = (1 - \exp(-L / \lambda_n))(e\dot{m} / M) / I_d \qquad (9)$$

Multiply-charged ionization, which happens in the case of the high electron temperature, is not considered in this equation, because the increase in multiply-charged ions leads to the increase in a frozen flow loss which is not a desirable condition. It would be better for the electron temperature to be kept below 20 eV. If the recombination reaction between the ions and electrons on the channel walls is taken into the model, β can be larger than the one in Eq. (9). However, it is neither not desirable because the increase in the wall-recombination rate implies the increase in the wall erosion and the energy dissipation rates.

Neutral mean free-path

The neutral mean free path is determined mainly from the operational conditions. The neutral particle velocity is assumed constant as

$$v_n = (1/4)\sqrt{3kT_n / M} \qquad (10)$$

The electron density can be estimated from the one-dimensional electron diffusion equation.

Neglecting the density gradient effect, the electron backstreaming current toward the anode is expressed by

$$I_e = en_e\mu(V_a/L)S \qquad (11)$$

If we assume the anomalous diffusion (Bohm diffusion), μ is identical to $1/16B$. Therefore, the electron density is written as

$$n_e = (16/e)(I_e/S)/(V_a/BL) \qquad (12)$$

Both I_e/S and V_a/BL are also the important design parameters. I_e/S is the electron current density in the channel, which prescribes the relationship between the input power and the thruster size. V_a/BL is a unique parameter for the Hall thruster operation, which is adjustable by changing the coil excitation current.

The collision frequency is a function of the electron temperature. The electron temperature varies in the channel from 5 to 20 eV. In this range of temperature, the collision frequency can be expressed by the equation

$$\langle\sigma v\rangle = \pi r_n^2\sqrt{\frac{8kT_e}{\pi m}}\left(1+\frac{eV_{ion}}{kT_e}\right)\exp\left(-\frac{eV_{ion}}{kT_e}\right) \qquad (13)$$

In order to find the electron temperature, an energy conservation model is needed. However, the electron temperature is thought one of the operating parameters which you can choose, because it must be a function of η_u and V_a. The calculated neutral mean-free path for xenon, krypton, and argon is shown in Fig. 9.

Optimum channel length

Substituting Eqs. (4) and (9) into Eq. (3), η_a is expressed by a function of a channel length as

$$\eta_a = \exp\left(-\frac{L}{\chi W}\right)\left(1-\exp\left(-\frac{L}{\lambda_n}\right)\right)\frac{(em/M)}{I_d} \qquad (14)$$

The efficiency should have a peak where its derivative becomes zero. The optimum channel length, L_{opt} is expressed by a following simple algebraic equation:

$$L_{opt} = \lambda_n \log(1+\chi W/\lambda_n) \qquad (15)$$

Figure 10 shows the theoretical optimum channel length calculated from Eq. (15). The optimum length increases with the increase in the ion mean free-path and then approaches to χW when the ion mean free-path becomes comparable to the channel width.

Figure 11 shows the optimum channel length for our typical experimental condition. As predicted from the experiments, the optimum length for xenon and krypton becomes less than 4 mm.

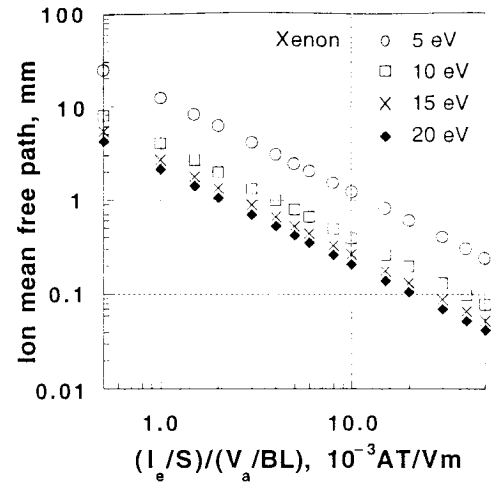

Fig. 9 (a) Ion mean free path for Xe

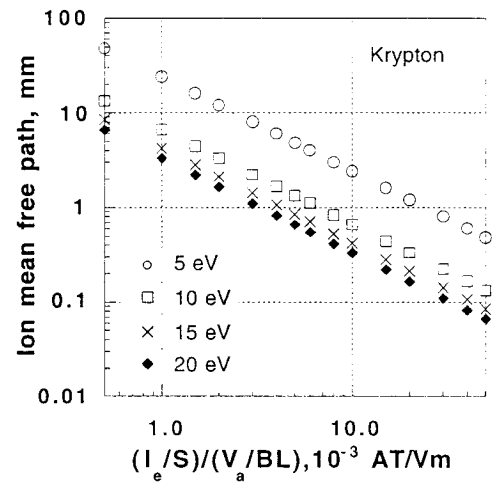

Fig. 9 (b) Ion mean free path for Kr

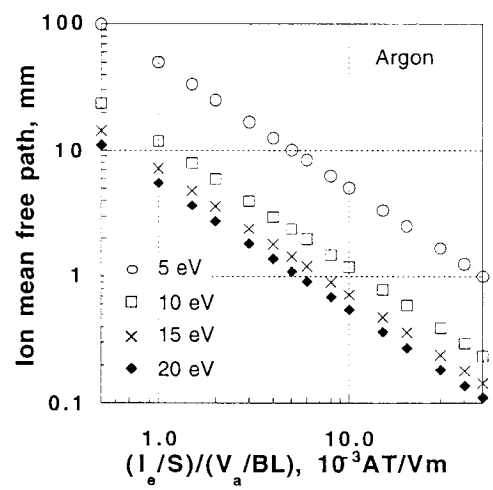

Fig. 9 (c) Ion mean free path for Ar

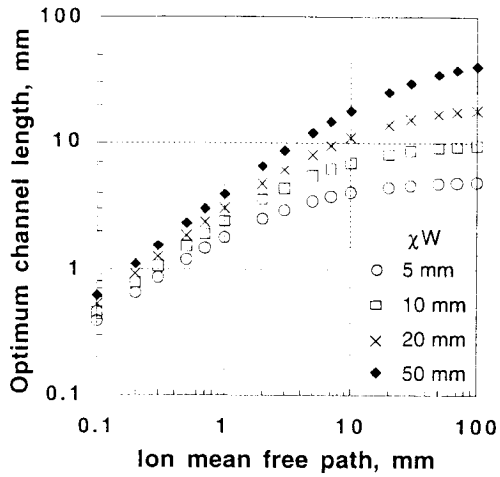

Fig. 10 Theoretical optimum channel length.

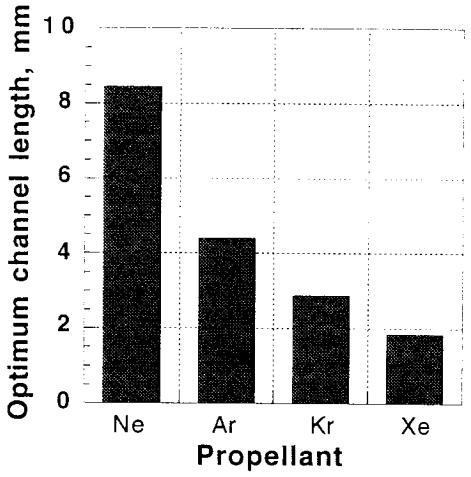

Fig. 11 Optimum channel length for the operating conditions in our experiments. I_e/S = 1 kA/m^2, V_a/BL = 50 kV/Tm, T_e = 5 eV, χW = 12 mm, T_n = 600 K

Summary

The ion-beam current extracted from a variable channel-length Hall thruster was measured for evaluating the thruster performance using a multi-ion-collector system. The total beam-ion current was obtained from the integration of the angular current-density distribution of the ion-beam with the compensation for the current-decrease due to the resonant charge exchange reaction in the vacuum chamber.

The measured acceleration efficiency had a peak at L = 4 mm when argon is used as a propellant. The optimum length did not change with the magnitude of the magnetic induction.

From a theoretical consideration, the optimum length was expressed by a function of the neutral mean free path and the channel width.

References

1) Brophy J.R., "Stationary Plasma Thruster Evaluation in Russia," JPL Publication 92-4, Summary Report, 1992.

2) Bober A., Maslennikov N., Day M., Popov G. and Rylov Yu., "Development and Application of Electric Propulsion Thruster in Russia," 23rd International Electric Propulsion Conference, IEPC 93-001, 1993.

3) Kahn J., Zhurin V., Kozubsky K., Randolph T. and Kim V., "Effect of Background Nitrogen and Oxygen on Insulator Erosion in the SPT-100," 23rd International Electric Propulsion Conference, IEPC 93-092, 1993.

4) Garner C.E., Polk J.E., Goodfellow K.D. and Brophy J.R., "Performance Evaluation and Life Testing of the SPT-100," 23rd International Electric Propulsion Conference, IEPC 93-091, 1993.

5) Semenkin A.V., "Investigation of Erosion in Anode Layer Thruster," 23rd International Electric Propulsion Conference, IEPC 93-231, 1993.

6) Absalamov S.K., Andreev V.B., T. Colbert, Day M., Egorov V.V., Gnizdor R.U., Kaufman H., Kim V., Korakin A.I., Kozbsky K.N., Kudravzev S.S, Lebedev U.V., Popov G.A. and Zhurin V.V., "Measurement of Plasma Parameters in the Stationary Plasma Thruster (SPT-100) Plume and Its effect on Space craft Components," 28th Joint Propulsion Conference and Exhibit, AIAA 92-3156, 1993.

7) Komurasaki K. and Arakawa Y., "Hall Ion-Thruster Performance," *Journal of Propulsion and Power*, Vol. 8, No. 6, 1992, pp. 1212-1216.

8) Komurasaki K., Hirakawa M. and Arakawa Y., "Plasma Acceleration Process in a Hall Thruster," 22rd International Electric Propulsion Conference, IEPC 91-078, 1991.

9) Komurasaki K. and Arakawa Y., "Two Dimensional Numerical Model of Plasma Flow in a Hall Thruster," *Journal of Propulsion and Power*, Vol. 11, No. 6, 1995.

10) Randolph T. Kim V., Kaufman H., Kozubsky K., Zhurin V. and Day M., "Facility effects on Stationary Plasma Thruster Testing," 23rd International Electric Propulsion Conference, IEPC 93-093, 1993.

11) Myes R.M. and Manzella D.H., "Stationary Plasma Thruster Plume Characteristics," 23rd International Electric Propulsion Conference, IEPC 93-096, 1993.

12) Pencil, E.J. "Preliminary Far-Field Plume Sputtering of the Stationary Plasma Thruster (SPT-100)," 23rd International Electric Propulsion Conference, IEPC 93-098, 1993.